

Light mesons in QCD and unquenching effects from the 3PI effective action

Richard Williams,^{1,*} Christian S. Fischer,^{1,†} and Walter Heupel^{1,‡}

¹*Institut für Theoretische Physik, Justus-Liebig-Universität Giessen, 35392 Giessen, Germany.*

We investigate the impact of unquenching effects on QCD Green's functions, in the form of quark-loop contributions to both the gluon propagator and three-gluon vertex, in a three-loop inspired truncation of the three-particle irreducible (3PI) effective action. The fully coupled system of Dyson-Schwinger equations for the quark-gluon-, ghost-gluon- and three-gluon vertices, together with the quark propagator, are solved self-consistently; our only input are the ghost and gluon propagators themselves that are constrained by calculations within Lattice QCD. We find that the two different unquenching effects have roughly equal, but opposite, impact on the quark-gluon vertex and quark propagator, with an overall negative impact on the latter. By taking further derivatives of the 3PI effective action, we construct the corresponding quark-antiquark kernel of the Bethe-Salpeter equation for mesons. The leading component is gluon exchange between two fully-dressed quark-gluon vertices, thus introducing for the first time an obvious scalar-scalar component to the binding. We gain access to time-like properties of bound-states by analytically continuing the coupled system of Dyson-Schwinger equations to the complex plane. We observe that the vector axial-vector splitting is in accord with experiment and that the lightest quark-antiquark scalar meson is above 1 GeV in mass.

PACS numbers: 12.38.Aw, 12.38.Lg, 14.40.-n

I. INTRODUCTION

The plethora of experimental phenomena related to the global properties and the internal structure of hadronic bound states and resonances are generated from the underlying non-perturbative interaction of quarks and gluons described by QCD. These relations can be made apparent using functional methods such as the framework of Dyson-Schwinger and Bethe-Salpeter equations or the functional renormalization group, see [1–6] for reviews.

One of the long-standing goals within the Dyson-Schwinger/Bethe-Salpeter framework is to establish robust truncation schemes that can be systematically applied to the calculation of bound-state properties. Such constructions can be approached from two different perspectives: bottom-up or top-down. While the former employs phenomenological input in order to construct models and constrain their parameters, the latter requires a robust theoretical foundation upon which to build [2]. Consequently there is a rich and diverse history regarding truncations, ranging from schemes that adhere to computational prudence [7, 8], set-ups that employ symmetries and identities to constrain Green's functions beyond propagators [9–11], to recent investigations wherein vertices are solved for explicitly [12–25].

Obtaining a suitable description of QCD within the functional approach is relevant for several diverse reasons. Aside from studying intrinsic properties of Green's functions and their connection to confinement, one can explore properties of the fundamental quark and gluon degrees of freedom in-medium, thus providing a handle

on the QCD phase diagram. Additionally, composite systems can be constructed in the form of mesons [26, 27], baryons [28, 29], glueballs [30] and tetraquarks [31, 32], with their mass spectra, decays and electromagnetic interactions explored [33–35]. This of course necessitates that key symmetries are maintained – a principle difficulty in constructing viable truncations – as we shall discuss later.

Furthermore, detailed Lattice calculations of QCD in Landau gauge are by now sufficiently advanced that they can serve to provide auxiliary information. This not only enables one to judge the efficacy of existing truncations, but to provide key ingredients or missing information. Finding coincidence or convergence between these complementary non-perturbative approaches enables hybrid constructions to be developed along the lines of Refs. [36, 37], wherein the difficulties of one approach (such as the sign problem) can be circumvented.

In this article, we explore one of the most important ingredients in non-perturbative studies of QCD that couple together the gauge and matter sector: the quark-gluon vertex. However, rather than following the customary approach of truncating the 1PI Dyson-Schwinger equations at the level of vertex functions, we take here a more pragmatic (and arguably more systematic) approach by truncating the n PI effective action to a given loop order. In particular, we take the 3PI effective action to three-loops, such that all two- and three-point functions are dynamical quantities. This is a natural step beyond the system explored in Ref. [38, 39] which is analogous to a three-loop truncation of the 2PI effective action. The resulting system of equations is still extremely complex and expensive in numerical terms, in particular due to the two-loop structure of the resulting Dyson-Schwinger equation (DSE) for the gluon propagator. We therefore solve the DSEs for the ghost and gluon propagator in

* richard.williams@physik.uni-giessen.de

† christian.fischer@physik.uni-giessen.de

‡ walter.heupel@physik.uni-giessen.de

a separate truncation providing solutions that are close to corresponding (quenched and unquenched) lattice results. These are then used as input into the remaining 3PI equations for the primitively divergent three-point vertices together with the quark propagator. We solve these self-consistently and discuss the impact of unquenching effects on the quark-gluon and three-gluon vertices. Finally, we apply our approach to the Bethe-Salpeter description of mesons and determine a number of observables consistent with the axial Ward-Takahashi identity. In general, our top-down approach is similar in spirit to a corresponding effort within the framework of the functional renormalization group [22, 23].

This paper is organized as follows. In section II we introduce in brief the 3PI effective action of QCD at three-loop order and present the relevant dynamical quantities, the propagators and vertices, together with their equations of motion in closed form. In section III we give our results for each Green's function and discuss the impact of quark-loops on the three-gluon vertex. We apply the formalism to the calculation of meson observables in a symmetry preserving truncation of the Bethe-Salpeter equation. In section IV we conclude; some technical details are relegated to an appendix.

II. FRAMEWORK

In the functional approach, the Dyson-Schwinger equations are the equations of motion corresponding to the 1PI effective action. They are comprised of coupled integral equations that form exact relations between the

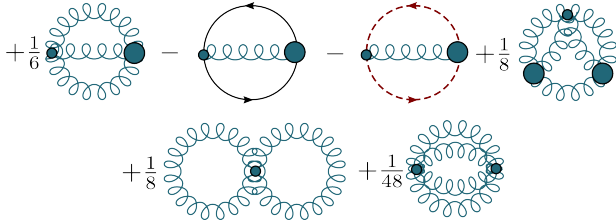


FIG. 1. Non-interacting part of the 3PI effective action, to three-loop. All propagators are considered dressed. Throughout the paper springs describe gluons, dashed lines Faddeev-Popov ghosts and solid lines quarks. Small filled circles describe bare and large filled circles describe dressed vertices.

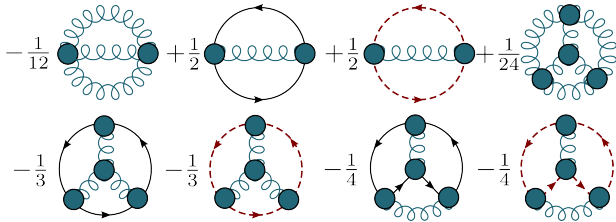


FIG. 2. Interacting part of the 3PI effective action, to three-loop.

theory's infinite tower of n -point Green's functions. The effective action, $\Gamma[\phi]$, is obtained from the generating functional of connected Green's functions $W[J]$ by a Legendre transform

$$\Gamma[\phi] = W[J] - J_i \phi_i, \quad (1)$$

from which n -point correlation functions are defined

$$G_{(n)}(p_1, \dots, p_n) = \frac{\delta^n \Gamma[\phi]}{\delta \phi_1 \dots \delta \phi_n}, \quad (2)$$

by taking functional derivatives. Then, the DSE for a 1PI Green's function can be derived from the functional identity

$$\frac{\delta \Gamma[\phi]}{\delta \phi_i} - \frac{\delta S}{\delta \phi_i} \left[\phi + \frac{\delta^2 W[J]}{\delta J \delta J_k} \frac{\delta}{\delta \phi_k} \right] = 0. \quad (3)$$

However, by themselves the DSEs do not form a closed system and require truncation. Typically this involves specifying the behavior of higher order n -point functions and collapsing the infinite tower to a manageable set of coupled equations.

Another approach is to work with a different resummation of the effective action by performing additional Legendre transformations of the action (1), this time with respect to propagators and vertices [40]. Here we consider the 3PI effective action which in compact notation [41–43] reads

$$\Gamma[\phi, D, U] = S_{cl}[\phi] + \frac{i}{2} \text{Tr} \text{Ln} D^{-1} + \frac{i}{2} \text{Tr} [D_{(0)}^{-1} D] - i\Phi^0[\phi, D, U] - i\Phi^{int}[\phi, D, U] + \text{const}. \quad (4)$$

The superfield ϕ represents all fields in the action, and D, U are the corresponding propagators and three-point vertices. As usual, the equations of motion are obtained by taking functional derivatives

$$\frac{\delta \Gamma[\phi, D, U]}{\delta D} = \frac{\delta \Gamma[\phi, D, U]}{\delta U} = 0. \quad (5)$$

The resulting set of equations for the propagators and vertices is then closed. In the case of QCD, the non-interacting part, $\Phi^0[\phi, D, U]$ is given in Fig. 1, and the interacting part $\Phi^{int}[\phi, D, U]$ in Fig. 2.

Note that throughout this paper we work in Euclidean space, wherein spacelike momenta are those for which $p^2 \geq 0$. To compute time-like properties of bound-states we must analytically continue to complex momenta; we will discuss this later in brief. For the sake of brevity we will drop the majority of (easily determinable) momentum arguments in the equations that follow.

A. Ghost and gluon propagators

The ghost propagator in Landau gauge is defined

$$D_G(p) = -\frac{G(p^2)}{p^2}, \quad (6)$$

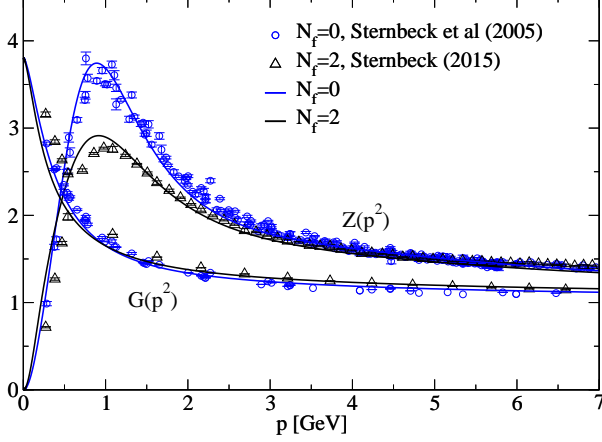


FIG. 3. Ghost and gluon dressing functions for the quenched ($N_f = 0$) and unquenched system ($N_f = 2$) compared with lattice data from Refs. [47, 48].

with $G(p^2)$ the ghost dressing function. Similarly, the gluon propagator is

$$D^{\mu\nu}(p) = T_{(p)}^{\mu\nu} D_Z(p^2) = T_{(p)}^{\mu\nu} \frac{Z(p^2)}{p^2}, \quad (7)$$

with $Z(p^2)$ a momentum dependent dressing function. The tensor structure is given by the transverse projector

$$T_{(p)}^{\mu\nu} = \delta^{\mu\nu} - \frac{p^\mu p^\nu}{p^2}. \quad (8)$$

From (4)–(5) and Figs. 1, 2 we can derive the (truncated) DSE for the ghost and gluon propagators, displayed in Fig. 13 in appendix A 1. Unfortunately, in contrast to the other DSEs considered in this work, these feature two-loop diagrams with squint and sunset topology that pose a significant calculational challenge. This prevents a complete self-consistent solution together with the DSEs for the vertices¹. On the other hand, we need quantitatively correct ghost and gluon propagators as input for the other DSEs we wish to solve, i.e. the one for the ghost-gluon vertex, the three-gluon vertex, the quark-gluon vertex and the quark.

To bypass this difficulty, we employ the framework of Refs. [15, 49, 50] and solve a coupled system of ghost, gluon and (in case of $N_f \neq 0$) quark propagators using model ansatzes for the three-point vertices, while neglecting all diagrams that involve the four-gluon vertex (i.e. the two-loop diagrams). The ansatzes are chosen such that lattice data for the ghost and gluon propagators for

$N_f = 0$ (quenched) and $N_f = 2$ (unquenched) quark flavors are reproduced. The advantages of this procedure over just using the lattice data for ghost and glue in the other DSEs are two-fold. First, we are able to use continuous solutions for the ghost and gluon propagators as input without the need to interpolate and extrapolate the lattice data. Second, we can set up and use a consistent renormalization scheme for all DSEs with appropriate renormalization factors $Z_3(\mu, \Lambda)$ and $\tilde{Z}_3(\mu, \Lambda)$ at a consistent renormalization point μ and numerical cutoff Λ . However, this comes at a price: neglecting the two-loop diagrams but still reproducing the results of the lattice calculations means that we have to use effective ghost-gluon, three-gluon and (to a lesser extent) quark-gluon vertex models in the ghost-gluon DSEs that make up for the neglected contributions. These are then no longer quantitatively consistent with the explicit vertices determined in this work.

Relegating all technical details to appendix A 1 we only discuss the resulting ghost and gluon dressing functions $G(p^2)$ and $Z(p^2)$ and compare them with corresponding lattice data in Fig. 3. In the figure, the data are taken from Ref. [47, 48]. Similar data from other groups have been discussed in Ref. [51, 52]. The agreement in the quenched case is almost perfect, and for the unquenched case is very good on the level of a few percent. This is certainly sufficient for our study.

B. Quark propagator

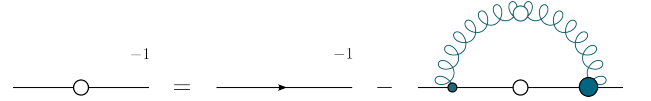


FIG. 4. Diagrammatic representation of the quark DSE. Blobs on propagators indicate they are dressed.

The quark propagator in vacuum has the general decomposition

$$S^{-1}(p) = Z_f^{-1}(p^2) [i\not{p} + M(p^2)], \quad (9)$$

where $Z_f(p^2)$ and $M(p^2)$ are the quark wave function and mass function, respectively. They are obtained by solving the quark gap equation, see Fig. 4, given by

$$S^{-1} = Z_2 S_{(0)}^{-1} + Z_{1f} C_F g_s^2 \int_k \gamma^\mu S \Gamma_{\text{qg}}^\nu D^{\mu\nu}, \quad (10)$$

with $\int_k = d^4k/(2\pi)^4$ the integration measure, $C_F = 4/3$ the result of the color trace, and $S_{(0)}^{-1}$ the bare inverse propagator. The quark and quark-gluon vertex renormalizations are Z_2 , Z_{1f} respectively. The quark-gluon vertex Γ_{qg}^ν is detailed in the next subsection.

¹ Though see [24, 44–46] for some progress within simpler truncation schemes.

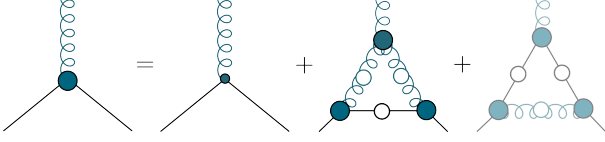


FIG. 5. Diagrammatic representation of the quark-gluon vertex DSE.

C. Quark-gluon vertex

The quark-gluon vertex can be decomposed into a set of Dirac-Lorentz covariants X_i^μ and scalar dressings h_i

$$\Gamma_{\text{qg}}^\mu(l, k) = \sum_i h_i X_i^\mu(l, k). \quad (11)$$

The covariants are any linear combination of the following twelve elements γ^μ , $\gamma^\mu \not{k}$, $\gamma^\mu \not{l}$, $\gamma^\mu \not{k} \not{l}$, k^μ , $k^\mu \not{k}$, $k^\mu \not{l}$, $k^\mu \not{k} \not{l}$, l^μ , $l^\mu \not{k}$, $l^\mu \not{l}$, $l^\mu \not{k} \not{l}$. In Landau gauge, however, it is more convenient to work with the transversely projected vertex where each element transforms correctly under charge conjugation. Just eight components suffice

$$\begin{aligned} T_{(k)}^{\mu\nu} \Gamma^\nu(l, k) = & h_1 \gamma_T^\mu + h_2 l_T^\mu \not{l} + h_3 i l_T^\mu \\ & + h_4 (l \cdot k) \frac{i}{2} [\gamma_T^\mu, \not{l}] + h_5 \frac{i}{2} [\gamma^\mu, \not{k}] \\ & + h_6 \frac{1}{6} \left\{ [\gamma^\mu, \not{l}] \not{k} + [\not{l}, \not{k}] \gamma^\mu + [\not{k}, \gamma^\mu] \not{l} \right\} \\ & + h_7 t_{(kl)}^{\mu\nu} (l \cdot k) \gamma^\nu + h_8 t_{(kl)}^{\mu\nu} \frac{i}{2} [\gamma^\nu, \not{l}]. \end{aligned} \quad (12)$$

Here, the incoming gluon momentum is k^μ , and l^μ is the relative quark momentum. Quantities with a subscript T are contracted with the transverse projector $T_{(k)}^{\mu\nu}$, see (8) and $\tau_{(kl)}^{\mu\nu} = (l \cdot k) \delta^{\mu\nu} - l^\mu k^\nu$.

The DSE for the vertex, following the three-loop truncation of the 3PI effective action, is given in Fig. 5. It consists of two vertex corrections which we refer to as the non-Abelian (since it involves gluon self-interaction) and Abelian diagrams

$$\Gamma_{\text{qg}}^\mu = Z_1 f \gamma^\mu + \Lambda_{\text{qg,NA}}^\mu + \Lambda_{\text{qg,AB}}^\mu. \quad (13)$$

Explicitly their contributions are

$$\Lambda_{\text{qg,NA}}^\mu = \frac{g_s^2 N_c}{2} \int_k \Gamma_{\text{qg}}^\alpha S \Gamma_{\text{qg}}^\beta \Gamma_{3\text{g}}^{\alpha\beta\mu} D_Z D_Z, \quad (14)$$

$$\Lambda_{\text{qg,AB}}^\mu = \frac{-g_s^2}{2N_c} \int_k \Gamma_{\text{qg}}^\alpha S \Gamma_{\text{qg}}^\mu S \Gamma_{\text{qg}}^\alpha D_Z. \quad (15)$$

Since the quark-gluon vertex is defined transverse with respect to its gluon momentum, it suffices to write only the scalar part of the gluon propagators, D_Z . Thus far the only component that has not been introduced is the three-gluon vertex $\Gamma_{3\text{g}}^{\mu\nu\rho}$, which we discuss later.

When solving the Abelian diagram, it is useful to make the substitution $\chi_{\text{qg}}^\mu = S \Gamma_{\text{qg}}^\mu S$, for the top-most vertex,

which significantly reduces the complexity of the resulting trace algebra. Despite the seeming complexity of the system, each iteration of the quark-gluon vertex takes about a minute on a standard desktop CPU.

D. Ghost-gluon vertex

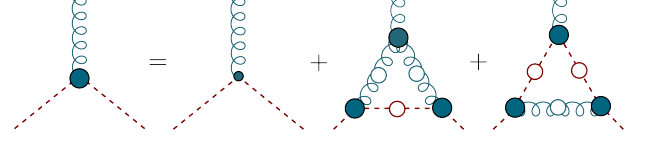


FIG. 6. Diagrammatic representation of the ghost-gluon vertex DSE.

For the ghost-gluon vertex in Landau gauge, there is just the one dressing function, $f(l, q)$ and corresponding tensor structure

$$\Gamma_{\text{gh}}^\mu(l, q) = f(l, q) T_{(q)}^{\mu\nu} l^\nu \quad (16)$$

with $l = (p_1 + p_2)/2$ the relative ghost momentum and q the gluon momentum. The DSE, given in Fig. 6, is similar in form to that of the quark-gluon vertex

$$\Gamma_{\text{gh}}^\mu = \tilde{Z}_1 l_T^\mu + \Lambda_{\text{gh,NA}}^\mu + \Lambda_{\text{gh,AB}}^\mu, \quad (17)$$

where $\tilde{Z}_1 = 1$ in Landau gauge. The individual contributions are given by

$$\Lambda_{\text{gh,NA}}^\mu = \frac{g_s^2 N_c}{2} \int_k \Gamma_{\text{gh}}^\alpha \Gamma_{3\text{g}}^{\alpha\beta\mu} \Gamma_{\text{gh}}^\beta D_Z D_Z D_G, \quad (18)$$

$$\Lambda_{\text{gh,AB}}^\mu = \frac{g_s^2 N_c}{2} \int_k \Gamma_{\text{gh}}^\alpha \Gamma_{\text{gh}}^\mu \Gamma_{\text{gh}}^\alpha D_G D_G D_Z. \quad (19)$$

This system is sufficiently simple that we make no further comment upon its solution here.

E. Three-gluon vertex

The DSE for the three-gluon vertex from the 3PI effective action to three-loop, shown in Fig. 7 is

$$\begin{aligned} \Gamma_{3\text{g}}^{\mu\nu\rho} = & Z_1 \Gamma_{3\text{g}(0)}^{\mu\nu\rho} \\ & + \Lambda_{3\text{g,GH}}^{\mu\nu\rho} + \Lambda_{3\text{g,GL}}^{\mu\nu\rho} + \Lambda_{3\text{g,SF}}^{\mu\nu\rho} + \Lambda_{3\text{g,QL}}^{\mu\nu\rho}, \end{aligned} \quad (20)$$

where $Z_1 = Z_3/\tilde{Z}_3$ is the three-gluon vertex renormalization constant. The components for the ghost-loop (GH),

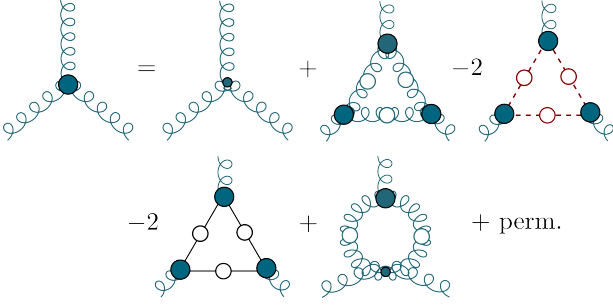


FIG. 7. Diagrammatic representation of the three-gluon vertex DSE. The last diagram containing a bare four-gluon vertex is cyclically permuted.

gluon-loop (GL), swordfish (SF) and quark-loop (QL) are

$$\Lambda_{3g, GH}^{\mu\nu\rho} = -N_C g_s^2 \int_q D_G D_G D_G \Gamma_{gh}^\rho \Gamma_{gh}^\nu \Gamma_{gh}^\mu, \quad (21)$$

$$\Lambda_{3g, GL}^{\mu\nu\rho} = \frac{N_C g_s^2}{2} \int_q D_Z D_Z D_Z \Gamma_{3g}^{\beta\alpha\rho} \Gamma_{3g}^{\alpha\gamma\rho} \Gamma_{3g}^{\gamma\beta\rho}, \quad (22)$$

$$\Lambda_{3g, SF}^{\mu\nu\rho} = -(3) \frac{3N_C g_s^2}{4} \int_q D_Z D_Z \Gamma_{3g}^{\beta\alpha\rho} \Gamma_{4g(0)}^{\mu\nu\beta\alpha}, \quad (23)$$

$$\Lambda_{3g, QL}^{\mu\nu\rho} = -\frac{g_s^2}{2} \sum_i \int_q \text{Tr} [\Gamma_{qg}^\rho S \Gamma_{qg}^\nu S \Gamma_{qg}^\mu S]. \quad (24)$$

The prefactors are the combination of symmetry factors (1/2 for the swordfish and 2 each for the ghost and quark loop) and color factors. The (3) for the swordfish denotes that there are three distinct permutations of the diagram that must be considered. Note also that the quark-loop contribution must be summed over each quark-flavor.

Following Ref. [18] where it was shown that the dominant tensor structure is the tree-level one, we use a reduced basis to describe the dressed three-gluon vertex

$$\Gamma_{3g}^{\mu\nu\rho}(p_1, p_2, p_3) = F_1 T_{(p_1)}^{\mu\alpha} T_{(p_2)}^{\nu\beta} T_{(p_3)}^{\rho\gamma} \Gamma_{3g(0)}^{\alpha\beta\gamma}(p_1, p_2, p_3), \quad (25)$$

with $F_1 = F_1(p_1^2, p_2^2, p_3^2)$. We can furthermore arrange p_1^2, p_2^2, p_3^2 into a set of S_3 permutation group variables, see Appendix A 2, and exploit the observation that $s_0 = (p_1^2 + p_2^2 + p_3^2)/6$ is the dominant variable. Finally,

$$\Gamma_{3g(0)}^{\alpha\beta\gamma}(p_1, p_2, p_3) = \delta^{\alpha\beta} (p_1 - p_2)^\gamma + \delta^{\beta\gamma} (p_2 - p_3)^\alpha + \delta^{\gamma\alpha} (p_3 - p_1)^\beta, \quad (26)$$

is the tree-level tensor structure of the three-gluon vertex.

III. RESULTS

All our calculations for the three-point functions are performed with full momentum dependencies. For the presentation of results, however, we concentrate on the

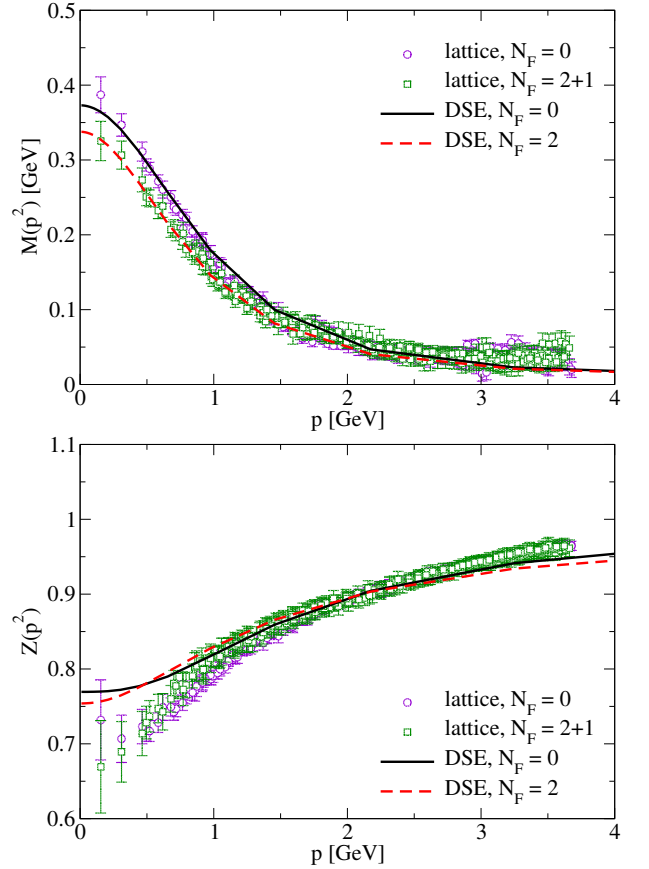


FIG. 8. The (top) quark mass function and (bottom) quark wave function calculated from the 3PI effective action, compared to quenched and unquenched Lattice data [53].

soft-gluon limit in which one gluon momentum is vanishing, $p_3 = 0$, whilst the remaining two legs carry the same momentum, $p_1 = p_2 = p$. This enables us to easily compare with existing and future lattice calculations. In terms of S_3 permutation group variables, this corresponds to the top of the Mandelstam triangle, see Fig. 14 in appendix A 2, with $s_0 = p^2/3$, $a = 0$, $s = 1$. For the three-gluon vertex, where the dressing function is near-independent of all but the variable $s_0 = (p_1^2 + p_2^2 + p_3^2)/6$, one may make use of s_0 and p interchangeably up to the obvious rescaling; this observation could be used to combine multiple phase space slices obtained on the lattice.

A. Quark Propagator

In Fig. 8 we show the quark mass function and wave function obtained from the three-loop truncation of the 3PI effective action. We show DSE results for the quenched and the unquenched case with $N_f = 2$. In the latter case quark loop effects in the ghost and gluon propagators as well as in the vertex-DSEs are taken into account. The DSE results are compared to quenched

and unquenched lattice calculations [53]. Note the unquenched lattice data is for $2 + 1$ flavors. However, since the majority of the unquenching effects stems from the two light quarks, the comparison is still meaningful. Within error bars, we find very good agreement between our results and the lattice data, with about the right size of unquenching effect seen in the mass function and still room for the inclusion of a third quark flavor as well as for additional unquenching effects. These may evolve e.g. from the inclusion of a pion cloud [54] and only become apparent at higher order than the 3PI truncation considered here. Note also that the wave function of the quenched propagator crosses that of the unquenched one, around $p = 0.4$ GeV. This is a feature suggested by the lattice data that has not been seen in a DSE study before. We attribute this feature to the interplay of the different tensor structures of the fully dressed quark-gluon vertex that is only accessible in a self-consistent diagrammatic calculation.

B. Quark-gluon vertex

In the following we report only results for the quark-gluon vertex upon neglecting the Abelian contribution; this is to provide consistency with the application to bound-states considered later, see section III E. We explicitly checked, however, that the inclusion of the Abelian contribution has very little impact on the system of propagators and vertices (on the level of few percent).

In the soft-gluon limit the quark gluon vertex reduces (after adapting to our conventions), to the form

$$\Gamma_{\text{qg}}^\mu(p, p, 0) = \lambda_1 \gamma^\mu - 4\lambda_2 \not{p}p^\mu + 2i\lambda_3 p^\mu, \quad (27)$$

where $\lambda_i = \lambda_i(p, p, 0)$. This is the usual Ball-Chiu construction of the vertex [55]. These dressing functions are related to those of our vertex in (12) by $\lambda_1 = h_1$, $\lambda_2 = -h_2/4$, and $\lambda_3 = h_3/2$.

In the top of Fig. 9 we show the result of our calculation of the quenched quark-gluon vertex, transformed to the Ball-Chiu basis and compared with the lattice data of Ref. [56]. While the λ_1 and λ_3 components are comparable (we introduced a vertical multiplicative shift in λ_1 to account for differences in the renormalization scheme), no agreement is seen in the λ_2 terms. This component is notoriously difficult to extract on the lattice (the product $4p^2\lambda_2$ should vanish at the origin) and consequently obtained large error bars. It remains to be seen whether future more precise lattice calculations still retain this discrepancy. In the bottom of Fig. 9 we show our result for the unquenched quark-gluon vertex for the basis employed in (12); for the purposes of plotting, we reversed the sign of the h_2 component. At present there are no available lattice data for the unquenched quark-gluon vertex with which to make a comparison. However, our results are not dissimilar to those reported in Ref. [20] which corresponds to a three-loop expansion of

the 2PI effective action. It would be interesting to compare with other truncations of the quark-gluon vertex in the DSE approach [24, 25] and from the functional renormalization group [22]. However, the results therein have not yet been reported in a form that enables us to easily make a direct comparison. This is therefore relegated to future work.

C. Ghost-gluon vertex

For completeness we determine the dressing of the ghost-gluon vertex, in spite of the deviation of its tree-level term being small in Landau gauge. The result, for both the quenched and unquenched systems, is shown in Fig. 10 and compared to extant lattice data. There is good agreement between our determination and that of the larger 48^4 lattice [57, 58], although clearly more work needs to be done to reduce the statistical errors. The impact of unquenching on the system is somewhat

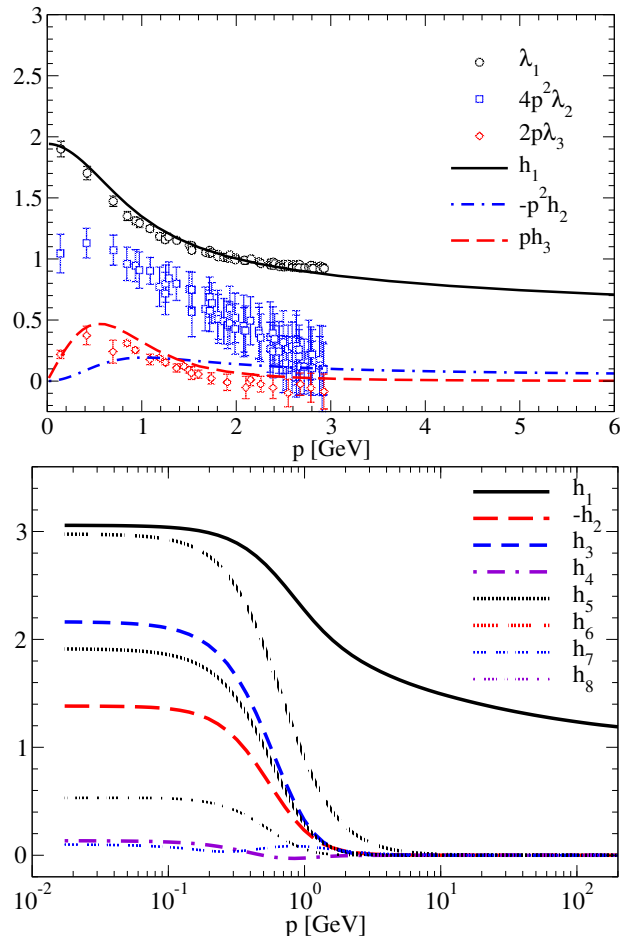


FIG. 9. (top) Calculated quark-gluon vertex compared to lattice calculations [56] in the soft-gluon limit for quenched QCD; (bottom) The components of our unquenched quark-gluon vertex, also in the soft-gluon limit (the quenched results are similar).

negligible; thus the oft-employed approximation that the ghost-gluon vertex can be taken bare remains a good one. Compared with previous DSE studies [15, 59], the deviation of our ghost-gluon vertex from one is a factor of 2 or 3 smaller, which is a result of the three-gluon vertex being dressed in the 3PI approach.

D. Three-gluon vertex

The leading component of the three-gluon vertex, for both quenched and unquenched configurations, is shown in the top panel of Fig. 11. In both cases, there is a zero crossing present below $p = 0.2$ GeV in the soft-gluon kinematics. This is too low to have a discernible impact on the properties of hadrons. Nevertheless, the strong running of the vertex from its ultraviolet perturbative momentum dependence down to values close to zero in the infrared clearly shows that the dynamics of this vertex is an important ingredient in any calculations and may not be neglected. Curiously, while the impact of quark-loops on the gluon propagator is a reduction in its strength (see Fig. A 1), the opposite appears true in the three-gluon vertex where unquenching effects are clearly additive², see the lower panel of Fig. 11.

In general, gluon propagators and three-gluon vertices appear in combinations on the right hand sides of the DSEs for the three-gluon and the quark-gluon vertex. Thus the unquenching effects in the gluon propagator compete against their sister contributions in the three-gluon vertex. Within the three-gluon vertex DSE we find

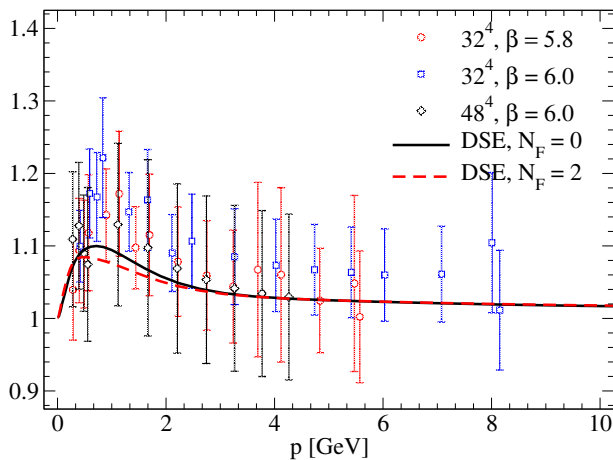


FIG. 10. The ghost-gluon vertex in the soft-gluon limit, as calculated from its DSE in (6). The data points correspond to lattice data from Refs. [57, 58].

² Note that this is in contradiction to the preliminary results reported in Ref. [60]. We attribute this to a potential global sign error in their quark loop contribution. We checked explicitly that our sign leads to the correct flavor dependence of the anomalous dimension of the vertex [61].

that unquenching in the three-gluon vertex wins – at least for two quark flavors – and consequently the unquenched three-gluon vertex is less suppressed, as compared to its tree-level value, than the quenched system. For this reason, unquenching effects in the gluon propagator and the three-gluon vertex partly balance each other also in the DSE for the quark-gluon vertex. Thus, the net unquenching effect on the quark-gluon vertex and quark mass function is not as dramatic as one may expect from the gluon propagator alone.

E. Application to bound-states

Before we present results for the bound-states, it is appropriate to discuss some of the implications of choosing the top-down approach wherein the emphasis is upon reproducing the Green's functions of QCD (i.e. those that are in agreement with lattice calculations). Since the system we consider is ultimately a truncation of the effective action it is not guaranteed that the resulting meson spectrum will be in agreement with experiment. That is, the scales inherited from the Lattice ghost and gluon propagators may not yield a phenomenologically precise value e.g. for the pion decay constant. Nonetheless, as the first work that incorporates a self-consistently solved 3PI-system including bound states, we choose the top-down approach and relegate a thorough discussion of the realisation of symmetry constraints and their impact on the low-lying meson/baryon spectrum to a future paper.

The Bethe-Salpeter kernel corresponding to the truncation at hand can readily be derived from the 3PI effective action [38, 40, 41, 62–64]. In the case of the Bethe-Salpeter equation (BSE) for a meson, its quark-antiquark kernel is obtained by twice differentiating with respect to the quark propagator S ; in Appendix A 3 we discuss how consistency with the axial-vector Ward-Takahashi identity leads to the appearance of a Goldstone boson in the chiral limit and the formation of the Gell-Mann-Oakes-Renner relation. The result, following simplification upon imposing the stationary condition, is given in Fig. 12 and features a one-gluon exchange contribution and a crossed-ladder exchange, with all propagators and vertices fully-dressed. Though the crossed-ladder diagram is N_c^2 suppressed with respect to the leading gluon exchange (similar to the Abelian vs. non-Abelian diagram in the quark-gluon vertex), it may yet be relevant due to the dynamical enhancement contained within the vertices. However, for reasons of expediency (i.e. to avoid a complicated two-loop term in the BS equation) we will not include the crossed-ladder term here. This can easily be made consistent at the level of the effective action by also dropping the corresponding diagram.

It follows that the Bethe-Salpeter equation is

$$\Gamma = C_F g_s^2 \int_k \Gamma_{qg}^\mu S T S T \Gamma_{qg}^\mu D_Z, \quad (28)$$

where once again we have omitted momentum arguments

for brevity. The quantum numbers of the amplitude under consideration, $\Gamma(p, P)$, are dictated by its tensor decomposition [26, 65, 66]. In a compact notation, we can solve this homogeneous equation

$$\Gamma_i = \lambda(P^2) K_{ij} \Gamma_j, \quad (29)$$

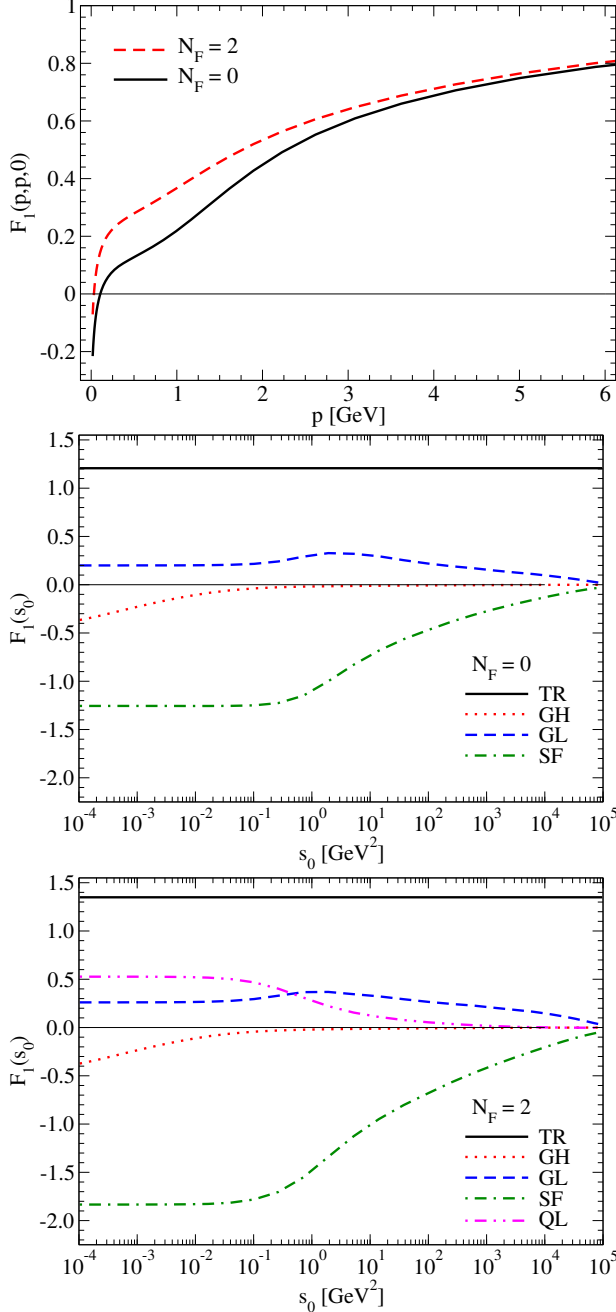


FIG. 11. (top) The three-gluon vertex, in the soft-gluon limit, for quenched vs unquenched QCD; Components contributing to the three-gluon vertex for quenched (middle) and unquenched (bottom) QCD. In the legend, we use abbreviations for tree-level (TR), ghost-loop (GH), gluon-loop (GL), sword-fish (SF) and quark-loop (QL).

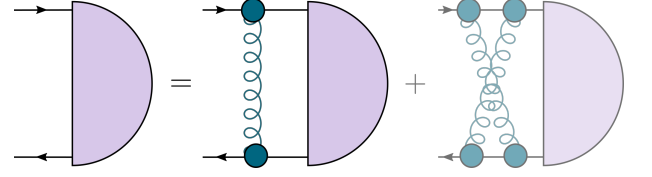


FIG. 12. Symmetry preserving Bethe-Salpeter equation corresponding to the truncation of the quark-gluon vertex in Fig. 5. The crossed ladder term, stemming from the abelian diagram in the vertex DSE, is displayed but discarded for the calculation of the bound-states.

TABLE I. Meson masses and pion decay constant in GeV as calculated in rainbow-ladder (RL) [68], the 2PI effective action at 3-loop (2PI-3L) [39] and in the 3PI effective action at 3-loop (3PI-3L) truncation as detailed here, compared to values from the Particle Data Group (PDG) [69]. Results affixed with † are fitted values.

	RL	2PI-3L	3PI-3L	PDG
$0^{-+} (\pi)$	0.14^\dagger	0.14^\dagger	0.14^\dagger	0.14
$0^{++} (\sigma)$	0.64	0.52	1.1(1)	0.48(8)
$1^{--} (\rho)$	0.74	0.77	0.74	0.78
$1^{++} (a_1)$	0.97	0.96	1.3(1)	1.23(4)
$1^{+-} (b_1)$	0.85	1.1	1.3(1)	1.23
f_π	0.092^\dagger	0.103	0.105	0.092

as an eigenvalue equation, where $\lambda(P^2) = 1$ gives solutions at discrete values of the bound-state total momentum squared, $P^2 = -M_i^2$. The matrix K_{ij} represents the integral kernel in the BSE.

As noted previously, access to time-like properties of bound-states (such as their masses), requires an analytic continuation to complex momenta. By carefully choosing the momentum routing, we can arrange the coupled system of DSEs to be such that only the quark and quark-gluon vertex need to be analytically continued to the complex plane. The subsequent evaluation of the quark and quark-gluon vertex is accomplished using a combination of the Cauchy contour method [50, 67], and the shell method [54]. Combining these two techniques together proves to be not only reliable, but also efficient.

The results of our calculation in the 3PI effective action at 3-loop (3PI-3L) are detailed in Table I and contrasted with typical results from rainbow-ladder (RL) [68], a recent study of mesons (and baryons) in the framework of the 2PI effective action at 3-loop (2PI-3L) [39], and of course their experimentally known values from the PDG [69]. We use the unquenched $N_F = 2$ system throughout.

We see that the pion appears as a pseudo-Goldstone boson in all truncations; its mass is fitted to 140 MeV in each case so as to determine the light quark mass used as input. As has been previously noted, that the system exhibits the correct chiral dynamics ensures that the mass of the vector meson is reproduced on the level of 5%.

One of the problems with the rainbow-ladder approach is its inability to reproduce the correct splitting of the axial-vectors and the ρ meson; that is, the axial-vectors are typically too light by several hundred MeV. This was partially remedied by including three-loop corrections in the 2PI effective action, lifting the size of one of the axial-vectors and thus suggesting that tensor structures in the quark-gluon vertex beyond the tree-level play an important role. Here, we find that the vector axial-vector splitting is $0.56(10)$ GeV for both charge conjugation states; this is of the same order as expected from experiment.

Similarly, whilst in RL and the 2PI-3L calculations there remains a light scalar around $0.5\text{--}0.6$ GeV (without a width) that complicates the interpretation of the $f_0(500)$ as a four-quark state [10], the present calculation lifts the lightest scalar to be $1.1(1)$ GeV in line with our expectations. These results agree with those of the bottom-up approach of [9], where an effective quark-gluon interaction is constructed to reproduce the vector axial-vector splitting with a heavy scalar. It will be interesting to see how our calculated top-down approach compares to the phenomenologically constrained one in detail.

Since the components of our 3PI quark-gluon vertex are similar to those of the 2PI-3L truncation, it appears that it is the difference in the structure of the kernel itself that leads to these improvements. Indeed, since the leading part of the kernel is a gluon-ladder that connects two fully-dressed quark-gluon vertices, we have for the first time included explicit scalar-scalar terms in addition to the usual vector-vector and, recently, vector-scalar ones considered thus far. It will be the topic of a future study to see how these effects impact upon the excited state spectrum, in particular that of charmonium, and what the consequences will be for baryons.

IV. CONCLUSION

We calculated the quark-gluon vertex in the three-loop truncation of the 3PI effective action, neglecting for now the backcoupling of the calculated vertices on the underlying ghost and gluon propagators, which are instead fixed separately such that agreement with the Lattice is obtained. We find that the leading part of the vertex is strongly enhanced for light quarks, as seen in previous studies, and that the sub-leading components are already quite stable in comparison to, for example, a 2PI truncation of the effective action to third loop order.

In addition, we investigated the impact of including unquenching effects in the form of quark-loop corrections to both the gluon propagators and three-gluon vertex. We find that they are sizeable in the latter, introducing a material shift in the location of the zero crossing to momenta deeper in the infrared. We also observed that the effects of unquenching in the three-gluon vertex act in opposition to those in the gluon propagator; as a consequence, the overall impact on the quark propagator and

quark-gluon vertex are smaller than one would naively expect.

By neglecting the Abelian contribution to the quark-gluon vertex – which by itself can be calculated without difficulty – we were able to apply the present framework to the calculation of quark-antiquark bound-states via the Bethe-Salpeter equations; the kernel of which was derived from the 3PI effective action and is used in accordance with the axial Ward-Takahashi identity to ensure the appearance of the pion as a Goldstone boson in the chiral limit. To obtain bound-state masses in the time-like region, we analytically continued the quark and quark-gluon vertices to complex momenta. In contrast to previous top-down studies we find that the lightest scalar is above 1 GeV, thus adding further evidence in support of the tetraquark picture of the $f_0(500)$ [31, 32], as well as reproducing the correct mass splitting between vector and axial-vector states.

To improve upon the present work, we would have to include solutions of the ghost and gluon propagators obtained self-consistently from the 3PI effective action. This would require that the inherent two-loop gluon polarizations be included. Additionally, the Abelian contribution to the quark-gluon vertex should be included with the difficult crossed-ladder term incorporated into the Bethe-Salpeter kernel. All of these tasks pose sizeable challenges – towards which we have made significant progress – and are thus relegated to a future work.

V. ACKNOWLEDGEMENTS

We thank G. Eichmann and H. Sanchis-Alepuz for useful discussions and a critical reading of this manuscript. We are grateful to Andre Sternbeck for sending us his lattice data for the unquenched gluon and ghost propagators prior to publication. This work has been supported by the Helmholtz International Center for FAIR within the LOEWE program of the State of Hesse and by BMBF under contract 06GI7121.

Appendix A: Technical Details

1. Ghost and gluon propagators

In the main text we explained the need to solve the DSEs for the quenched and unquenched ghost and gluon propagators using effective three-point vertices that incorporate the missing two-loop diagrams in the gluon DSE. The resulting system of equations is shown in Fig. 13. Here, we specify the vertex models used to solve this system of equations as well as the corresponding renormalization conditions. We choose $\alpha(\mu^2) = 0.124$ at the renormalization point $\mu = 57$ GeV together with the MiniMOM condition for the renormalization factor of the ghost-gluon vertex, $\tilde{Z}_1 = 1$ [70]. Moreover, we need to single out one instance of the one-parameter family of

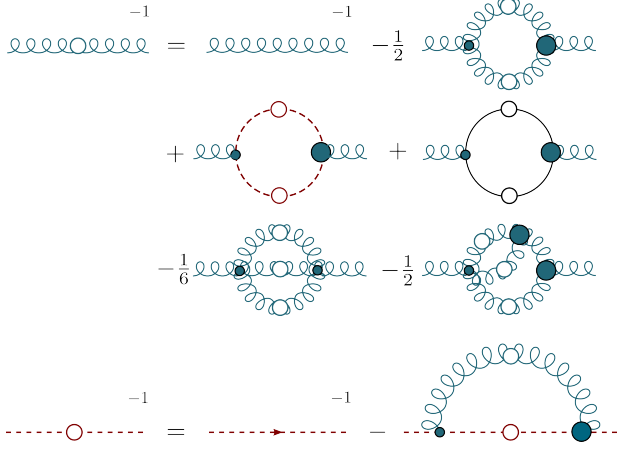


FIG. 13. The DSEs for the ghost and gluon propagators. In our truncation we neglect any contributions from the four-gluon vertex, i.e. the two-loop graphs are not included.

decoupling solutions, see Refs. [71, 72] for details. This is done by imposing the condition $G(0) = 3.8$ on the ghost dressing. These coupling and renormalization constants are carried over to the whole system of DSEs that are solved in the main body of this work, where the calculated ghost and gluon propagators serve as input.

For the ghost-gluon vertex model we use the simplest possible choice: the bare vertex. This choice is well justified in Landau gauge, as also discussed in the main text. For the three-gluon vertex we use the Bose-symmetric model suggested by Huber and Smekal in Ref. [15]

$$\Gamma_{3g}^{\mu\nu\rho}(p_1, p_2, p_3) = Z_1^{-1} \Gamma_{3g,0}^{\mu\nu\rho} D^{A^3,UV}(p_1, p_2, p_3) D^{A^3}(p_1, p_2, p_3), \quad (A1)$$

$$D^{A^3,UV}(p_1, p_2, p_3) = [G(3s_0)]^{3+1/\delta}, \quad (A2)$$

$$D^{A^3}(p_1, p_2, p_3) = D^{A^3,UV}(p_1, p_2, p_3) + D^{A^3,IR}(p_1, p_2, p_3), \quad (A3)$$

$$D^{A^3,IR}(p_1, p_2, p_3) = h_{IR} [G(6s_0)]^3 [f^{3g}(p_1^2) f^{3g}(p_2^2) f^{3g}(p_3^2)]^4. \quad (A4)$$

Here $s_0 = (p_1^2 + p_2^2 + p_3^2)/6$ parametrizes the leading scale dependence, and $f^{3g}(x) = (1 + x/\Lambda_{3g}^2)^{-1}$ is an infrared damping factor. The tensor structure of the bare three-gluon vertex is $\Gamma_{3g,0}^{\mu\nu\rho}$, the vertex renormalization factor is Z_1 , and $\delta = -9N_c/(44N_c - 8N_f)$ is the anomalous dimension of the ghost. The contribution $D^{A^3,UV}$ ensures the correct ultraviolet running of the vertex and $D^{A^3,IR}$ its damping in the infrared in agreement with the lattice data of the vertex and the numerical results, cf. [17, 18, 73] and our results in the main body of this work. The damping is controlled by two parameters, h_{IR} , Λ_{3g} , for which we choose $h_{IR} = -1$, $\Lambda_{3g} = 1.3$ GeV in the quenched case and in accordance with [15]. For the unquenched calculation ($N_f = 2$) we had to modify these values to $h_{IR} = -0.1$, $\Lambda_{3g} = 3.6$ GeV. Interestingly, these changes are qualitatively in agreement with the corresponding changes in our numerical results for the three-gluon vertex from its 3PI-DSE, discussed in section III D.

and gluon momentum p_3 it reads:

$$\Gamma_{qg}^\mu(p_1, p_2, p_3) = \gamma^\mu A(p_3^2) G^2(p_3^2) \tilde{Z}_3 \frac{(G(p_3^2) \tilde{Z}_3)^{-2d-d/\delta}}{(Z(p_3^2) Z_3)^d}. \quad (A5)$$

The construction is such that the ultraviolet momentum running of the vertex is the same for all values of the parameter d , leading to the correct ultraviolet running of the quark propagator in agreement with resummed perturbation theory. For our two-flavor calculations we choose $d = 1^3$. It has been noted already in Ref. [49, 50] that such a vertex model needs to have different momentum assignments when employed in the quark DSE and in the quark-loop of the gluon DSE. This can be shown strictly using multiplicative renormalisability. Thus we

For the quark-gluon vertex we employ a vertex ansatz that has been introduced in Ref. [49, 50] and is constructed along the (leading part) of the Slavnov-Taylor identity for the vertex. With quark momenta p_1 and p_2

³ Note that previous unquenched calculations of ghost and gluon propagators with the so-called scaling infrared behaviour resulted in values of d around $d = 0$ [49]. With decoupling, as adopted here, this value changes substantially.

use

$$\Gamma_{\text{qg}}^\mu(p_1, p_2, p_3) = \gamma^\mu \frac{A(p_1^2) + A(p_2^2)}{2} G(p_1^2) G(p_2^2) \times \tilde{Z}_3 \frac{(G(p_1^2)G(p_2^2))^{-d-d/(2\delta)} \tilde{Z}_3^{-2d-d/\delta}}{(Z(p_1^2)Z(p_2^2))^{d/2} Z_3^d}, \quad (\text{A6})$$

in the quark loop which leads to the correct running of the ghost and gluon propagators in the ultraviolet momentum region.

Finally we need to specify the bare quark masses for the two light quarks. Here we chose two chiral quarks for simplicity. We explicitly checked that only very tiny changes result for the ghost and gluon propagators when these values are modified to ones in the physical range, i.e. those that lead to the experimental pion mass.

2. Phase space and vertices: S_3 permutation group

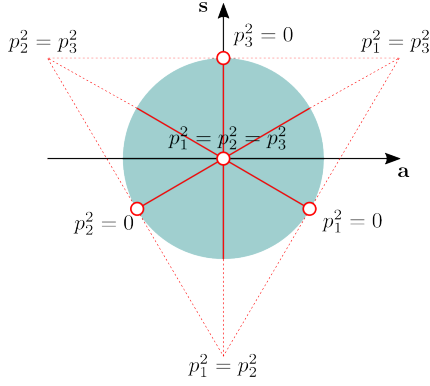


FIG. 14. Permutation group variables arranged into a Mandelstam plane.

Useful in the study of three-point functions is the expression of momenta p_1 , p_2 and p_3 in accord to the S_3 permutation group. Whilst this is of direct relevance for the three-gluon vertex [18], owing to bose-symmetry, it remains a useful representation also for both the ghost-gluon and quark-gluon vertices. In all cases, we arrange the momenta into the variables

$$s_0 = \frac{p_1^2 + p_2^2 + p_3^2}{6}, \quad (\text{A7})$$

$$a = \frac{\sqrt{3}(p_2^2 - p_1^2)}{6s_0}, \quad (\text{A8})$$

$$s = \frac{p_1^2 + p_2^2 - 2p_3^2}{6s_0}. \quad (\text{A9})$$

It is straightforward to see that the doublet (a, s) forms the inside of a circle, see Fig. 14, whilst the singlet s_0 carries an overall momentum scale. For actual calculations, instead of (a, s) a more natural parametrization of the circle in the polar coordinates (r, ψ) is chosen.

Consequently, symmetry properties of the vertex (provided a suitable basis is constructed) are reflected in the phase space variables. For example, bose-symmetry of the three-gluon vertex manifests as a $2\pi/3$ periodicity in the angular variables ψ . For the quark-gluon vertex (ghost-gluon vertex), charge conjugation (bose-symmetry in the ghost legs) manifests as reflection symmetry in the s -axis.

3. Axial Ward-Takahashi identity

In order for the system to feature a massless pion in the chiral limit and in the presence of dynamical chiral symmetry breaking, the interaction kernel of the Bethe-Salpeter equation and the self-energy of the quark must obey the axial-vector Ward-Takahashi identity. In the framework of Dyson-Schwinger and Bethe-Salpeter equations, this relation reads [74]

$$\frac{\delta^2 \Gamma}{\delta S \delta S} \{\gamma_5, S\} = 0, \quad (\text{A10})$$

where the curly brackets indicate an anti-commutator. For a given effective action Γ , it is sufficient that the effective action is invariant under a global chiral transformation⁴; for the 3PI effective action used in this work, chiral symmetry appears to be invariant by inspection. What is not obvious is the mechanism by which the invariance of the action is connected to the existence of a Goldstone boson. Following the steps in Ref. [74], we start with the global chiral transformation properties of the quark S and the quark-gluon vertex Γ_{qg}^μ

$$S' = e^{i\gamma_5 \tau^l \theta} S e^{i\gamma_5 \tau^l \theta}, \quad (\text{A11})$$

$$\Gamma_{\text{qg}}^{\mu'} = e^{-i\gamma_5 \tau^l \theta} \Gamma_{\text{qg}}^\mu e^{-i\gamma_5 \tau^l \theta},$$

where τ^l is a generator of the flavor group and θ is the real transformation angle. We checked explicitly that the quark DSE and vertex DSE are indeed invariant under such a *combined* transformation. Performing an infinitesimal chiral transformation of the effective action, which is zero by invariance, and subsequently taking a derivative with respect to the quark, the following relation is obtained

$$\frac{\delta^2 \Gamma}{\delta S \delta S} \{\gamma_5, S\} - \frac{\delta^2 \Gamma}{\delta S \delta \Gamma_{\text{qg}}^\mu} \{\gamma_5, \Gamma_{\text{qg}}^\mu\} = 0, \quad (\text{A12})$$

where for brevity we have dropped all indices and momentum/space-time arguments. The first term is the sought after Goldstone boson, where the anti-commutator is the wave function of the pion and the

⁴ See however Refs. [75, 76] in the case where chiral symmetry is broken by truncation artifacts.

second derivative of the effective action represents the BSE-operator. Thus, at first glance glance the second term seems to spoil the existence of a Goldstone boson. However, after a lengthy calculation that repeatedly employs the equation of motion of the quark-gluon vertex (see Fig. 5) and the constraint imposed by the axial Ward

identity, the following can be shown

$$\frac{\delta^2 \Gamma}{\delta S \delta S} \{\gamma_5, S\} = 0. \quad (\text{A13})$$

Thus, the truncated 3PI system features a massless pion. Further details of the systematics involved in this derivation will be given in a separate publication.

-
- [1] C. D. Roberts and A. G. Williams, *Prog. Part. Nucl. Phys.* **33**, 477 (1994), [arXiv:hep-ph/9403224 \[hep-ph\]](#).
 - [2] R. Alkofer and L. von Smekal, *Phys. Rept.* **353**, 281 (2001), [arXiv:hep-ph/0007355 \[hep-ph\]](#).
 - [3] C. S. Fischer, *J. Phys.* **G32**, R253 (2006), [arXiv:hep-ph/0605173 \[hep-ph\]](#).
 - [4] A. Bashir, L. Chang, I. C. Cloet, B. El-Bennich, Y.-X. Liu, C. D. Roberts, and P. C. Tandy, *Commun. Theor. Phys.* **58**, 79 (2012), [arXiv:1201.3366 \[nucl-th\]](#).
 - [5] J. Berges, N. Tetradis, and C. Wetterich, *Phys. Rept.* **363**, 223 (2002), [arXiv:hep-ph/0005122 \[hep-ph\]](#).
 - [6] J. M. Pawłowski, *Annals Phys.* **322**, 2831 (2007), [arXiv:hep-th/0512261 \[hep-th\]](#).
 - [7] H. J. Munczek and A. M. Nemirovsky, *Phys. Rev.* **D28**, 181 (1983).
 - [8] H. L. L. Roberts, A. Bashir, L. X. Gutierrez-Guerrero, C. D. Roberts, and D. J. Wilson, *Phys. Rev.* **C83**, 065206 (2011), [arXiv:1102.4376 \[nucl-th\]](#).
 - [9] L. Chang and C. D. Roberts, *Phys. Rev.* **C85**, 052201 (2012), [arXiv:1104.4821 \[nucl-th\]](#).
 - [10] W. Heupel, T. Goecke, and C. S. Fischer, *Eur. Phys. J.* **A50**, 85 (2014), [arXiv:1402.5042 \[hep-ph\]](#).
 - [11] A. C. Aguilar, D. Binosi, D. Ibañez, and J. Papavassiliou, *Phys. Rev.* **D90**, 065027 (2014), [arXiv:1405.3506 \[hep-ph\]](#).
 - [12] W. Schleifenbaum, A. Maas, J. Wambach, and R. Alkofer, *Phys. Rev.* **D72**, 014017 (2005), [arXiv:hep-ph/0411052 \[hep-ph\]](#).
 - [13] C. Kellermann and C. S. Fischer, *Phys. Rev.* **D78**, 025015 (2008), [arXiv:0801.2697 \[hep-ph\]](#).
 - [14] R. Alkofer, C. S. Fischer, F. J. Llanes-Estrada, and K. Schwenzer, *Annals Phys.* **324**, 106 (2009), [arXiv:0804.3042 \[hep-ph\]](#).
 - [15] M. Q. Huber and L. von Smekal, *JHEP* **04**, 149 (2013), [arXiv:1211.6092 \[hep-th\]](#).
 - [16] A. C. Aguilar, D. Binosi, D. Ibañez, and J. Papavassiliou, *Phys. Rev.* **D89**, 085008 (2014), [arXiv:1312.1212 \[hep-ph\]](#).
 - [17] A. Blum, M. Q. Huber, M. Mitter, and L. von Smekal, *Phys. Rev.* **D89**, 061703 (2014), [arXiv:1401.0713 \[hep-ph\]](#).
 - [18] G. Eichmann, R. Williams, R. Alkofer, and M. Vujanovic, *Phys. Rev.* **D89**, 105014 (2014), [arXiv:1402.1365 \[hep-ph\]](#).
 - [19] A. K. Cyrol, M. Q. Huber, and L. von Smekal, *Eur. Phys. J.* **C75**, 102 (2015), [arXiv:1408.5409 \[hep-ph\]](#).
 - [20] R. Williams, *Eur. Phys. J.* **A51**, 57 (2015), [arXiv:1404.2545 \[hep-ph\]](#).
 - [21] M. Vujanovic and R. Williams, *Eur. Phys. J.* **C75**, 100 (2015), [arXiv:1411.7619 \[hep-ph\]](#).
 - [22] M. Mitter, J. M. Pawłowski, and N. Strodthoff, *Phys. Rev.* **D91**, 054035 (2015), [arXiv:1411.7978 \[hep-ph\]](#).
 - [23] J. Braun, L. Fister, J. M. Pawłowski, and F. Rennecke, (2014), [arXiv:1412.1045 \[hep-ph\]](#).
 - [24] M. Hopfer, *Gauge Theories: QCD and Beyond*, Ph.D. thesis, Graz U. (2014).
 - [25] A. Windisch, *Features of strong quark correlations at vanishing and non-vanishing density*, Ph.D. thesis, Graz U. (2014).
 - [26] C. S. Fischer, S. Kubrak, and R. Williams, *Eur. Phys. J.* **A50**, 126 (2014), [arXiv:1406.4370 \[hep-ph\]](#).
 - [27] T. Hilger, M. Gomez-Rocha, and A. Krassnigg, (2015), [arXiv:1508.07183 \[hep-ph\]](#).
 - [28] G. Eichmann, R. Alkofer, A. Krassnigg, and D. Nicmorus, *Phys. Rev. Lett.* **104**, 201601 (2010), [arXiv:0912.2246 \[hep-ph\]](#).
 - [29] H. Sanchis-Alepuz, G. Eichmann, S. Villalba-Chavez, and R. Alkofer, *Phys. Rev.* **D84**, 096003 (2011), [arXiv:1109.0199 \[hep-ph\]](#).
 - [30] H. Sanchis-Alepuz, C. S. Fischer, C. Kellermann, and L. von Smekal, *Phys. Rev.* **D92**, 034001 (2015), [arXiv:1503.06051 \[hep-ph\]](#).
 - [31] W. Heupel, G. Eichmann, and C. S. Fischer, *Phys. Lett.* **B718**, 545 (2012), [arXiv:1206.5129 \[hep-ph\]](#).
 - [32] G. Eichmann, C. S. Fischer, and W. Heupel, *Phys. Lett.* **B753**, 282 (2016), [arXiv:1508.07178 \[hep-ph\]](#).
 - [33] P. Maris and P. C. Tandy, *Phys. Rev.* **C61**, 045202 (2000), [arXiv:nucl-th/9910033 \[nucl-th\]](#).
 - [34] G. Eichmann, *Phys. Rev.* **D84**, 014014 (2011), [arXiv:1104.4505 \[hep-ph\]](#).
 - [35] H. Sanchis-Alepuz, R. Williams, and R. Alkofer, *Phys. Rev.* **D87**, 096015 (2013), [arXiv:1302.6048 \[hep-ph\]](#).
 - [36] C. S. Fischer and J. Luecker, *Phys. Lett.* **B718**, 1036 (2013), [arXiv:1206.5191 \[hep-ph\]](#).
 - [37] C. S. Fischer, J. Luecker, and C. A. Welzbacher, *Phys. Rev.* **D90**, 034022 (2014), [arXiv:1405.4762 \[hep-ph\]](#).
 - [38] H. Sanchis-Alepuz and R. Williams, *Proceedings, 4th Symposium on Prospects in the Physics of Discrete Symmetries (DISCRETE 2014)*, *J. Phys. Conf. Ser.* **631**, 012064 (2015), [arXiv:1503.05896 \[hep-ph\]](#).
 - [39] H. Sanchis-Alepuz and R. Williams, *Phys. Lett.* **B749**, 592 (2015), [arXiv:1504.07776 \[hep-ph\]](#).
 - [40] J. M. Cornwall, R. Jackiw, and E. Tomboulis, *Phys. Rev.* **D10**, 2428 (1974).
 - [41] M. E. Carrington and Y. Guo, *Phys. Rev.* **D83**, 016006 (2011), [arXiv:1010.2978 \[hep-ph\]](#).
 - [42] M. C. A. York, G. D. Moore, and M. Tassler, *JHEP* **06**, 077 (2012), [arXiv:1202.4756 \[hep-ph\]](#).
 - [43] M. E. Carrington, W. Fu, T. Fugleberg, D. Pickering, and I. Russell, *Phys. Rev.* **D88**, 085024 (2013), [arXiv:1310.3295 \[hep-ph\]](#).

- [44] J. C. R. Bloch, *Few Body Syst.* **33**, 111 (2003), [arXiv:hep-ph/0303125 \[hep-ph\]](#).
- [45] J. Meyers and E. S. Swanson, *Phys. Rev.* **D90**, 045037 (2014), [arXiv:1403.4350 \[hep-ph\]](#).
- [46] V. Mader, *Signals of Confinement in the Dyson-Schwinger Equation for the Gauge Boson Propagator*, Ph.D. thesis, Graz U. (2014), [arXiv:1412.6348 \[hep-th\]](#).
- [47] A. Sternbeck, E. M. Ilgenfritz, M. Muller-Preussker, and A. Schiller, *Phys. Rev.* **D72**, 014507 (2005), [arXiv:hep-lat/0506007 \[hep-lat\]](#).
- [48] A. Sternbeck, private communication; in preparation.
- [49] C. S. Fischer and R. Alkofer, *Phys. Rev.* **D67**, 094020 (2003), [arXiv:hep-ph/0301094 \[hep-ph\]](#).
- [50] C. S. Fischer, P. Watson, and W. Cassing, *Phys. Rev.* **D72**, 094025 (2005), [arXiv:hep-ph/0509213 \[hep-ph\]](#).
- [51] A. Cucchieri and T. Mendes, *Phys. Rev. Lett.* **100**, 241601 (2008), [arXiv:0712.3517 \[hep-lat\]](#).
- [52] A. Ayala, A. Bashir, D. Binosi, M. Cristoforetti, and J. Rodriguez-Quintero, *Phys. Rev.* **D86**, 074512 (2012), [arXiv:1208.0795 \[hep-ph\]](#).
- [53] P. O. Bowman, U. M. Heller, D. B. Leinweber, M. B. Parappilly, A. G. Williams, and J.-b. Zhang, *Phys. Rev.* **D71**, 054507 (2005), [arXiv:hep-lat/0501019 \[hep-lat\]](#).
- [54] C. S. Fischer, D. Nickel, and R. Williams, *Eur. Phys. J.* **C60**, 47 (2009), [arXiv:0807.3486 \[hep-ph\]](#).
- [55] J. S. Ball and T.-W. Chiu, *Phys. Rev.* **D22**, 2542 (1980).
- [56] J. I. Skullerud, P. O. Bowman, A. Kizilersu, D. B. Leinweber, and A. G. Williams, *JHEP* **04**, 047 (2003), [arXiv:hep-ph/0303176 \[hep-ph\]](#).
- [57] E. M. Ilgenfritz, M. Muller-Preussker, A. Sternbeck, A. Schiller, and I. L. Bogolubsky, *Infrared QCD in Rio: Propagators, condensates and topological effects. Proceedings, International Meeting, IRQCD 2006, Rio de Janeiro, Brazil, June 5-9, 2006*, *Braz. J. Phys.* **37**, 193 (2007), [arXiv:hep-lat/0609043 \[hep-lat\]](#).
- [58] A. Sternbeck, *The Infrared behavior of lattice QCD Green's functions*, Ph.D. thesis, Humboldt U., Berlin (2006), [arXiv:hep-lat/0609016 \[hep-lat\]](#).
- [59] A. C. Aguilar, D. Ibáñez, and J. Papavassiliou, *Phys. Rev.* **D87**, 114020 (2013), [arXiv:1303.3609 \[hep-ph\]](#).
- [60] A. L. Blum, R. Alkofer, M. Q. Huber, and A. Windisch, *Proceedings, International Meeting of Excited QCD 2015*, *Acta Phys. Polon. Supp.* **8**, 321 (2015), [arXiv:1506.04275 \[hep-ph\]](#).
- [61] P. Pascual and R. Tarrach, *Lect. Notes Phys.* **194**, 1 (1984).
- [62] R. Fukuda, *Prog. Theor. Phys.* **78**, 1487 (1987).
- [63] M. Komachiya, M. Ukita, and R. Fukuda, *Phys. Rev.* **D40**, 2654 (1989).
- [64] D. W. McKay and H. J. Munczek, *Phys. Rev.* **D40**, 4151 (1989).
- [65] C. H. Llewellyn-Smith, *Annals Phys.* **53**, 521 (1969).
- [66] A. Krassnigg and M. Blank, *Phys. Rev.* **D83**, 096006 (2011), [arXiv:1011.6650 \[hep-ph\]](#).
- [67] A. Krassnigg, *Proceedings, 8th Conference on Quark Confinement and the Hadron Spectrum (Confinement8)*, PoS **CONFINEMENT8**, 075 (2008), [arXiv:0812.3073 \[nucl-th\]](#).
- [68] P. Maris and P. C. Tandy, *Phys. Rev.* **C60**, 055214 (1999), [arXiv:nucl-th/9905056 \[nucl-th\]](#).
- [69] K. A. Olive *et al.* (Particle Data Group), *Chin. Phys.* **C38**, 090001 (2014).
- [70] L. von Smekal, K. Maltman, and A. Sternbeck, *Phys. Lett.* **B681**, 336 (2009), [arXiv:0903.1696 \[hep-ph\]](#).
- [71] P. Boucaud, J. P. Leroy, A. Le Yaouanc, J. Micheli, O. Pene, and J. Rodriguez-Quintero, *JHEP* **06**, 099 (2008), [arXiv:0803.2161 \[hep-ph\]](#).
- [72] C. S. Fischer, A. Maas, and J. M. Pawłowski, *Annals Phys.* **324**, 2408 (2009), [arXiv:0810.1987 \[hep-ph\]](#).
- [73] A. Cucchieri, A. Maas, and T. Mendes, *Phys. Rev.* **D77**, 094510 (2008), [arXiv:0803.1798 \[hep-lat\]](#).
- [74] H. J. Munczek, *Phys. Rev.* **D52**, 4736 (1995), [arXiv:hep-th/9411239 \[hep-th\]](#).
- [75] A. Pilaftsis and D. Teresi, *Nucl. Phys.* **B874**, 594 (2013), [arXiv:1305.3221 \[hep-ph\]](#).
- [76] M. J. Brown and I. B. Whittingham, *Phys. Rev.* **D91**, 085020 (2015), [arXiv:1502.03640 \[hep-th\]](#).